MAGNETIC MEASUREMENTS OF INSERTION DEVICES USING THE VIBRATING WIRE TECHNIQUE

C. Baribeau[†], D. Bertwistle, E. Ericson, J. Gilbert, T. Pedersen, Canadian Light Source, University of Saskatchewan, 44 Innovation Boulevard, Saskatoon, Saskatchewan, S7N 2V3, Canada

Abstract

The commissioning of new in-vacuum insertion devices (ID) at the Canadian Light Source has motivated the assembly and development of a vibrating wire system. The advantage of the technique is that it is a sensitive magnetic measurement instrument at relatively low cost. Moreover, most Hall probe systems require transverse access, which is often not available for in-vacuum or Delta-like devices. It is comparatively simple to string a taut wire through the gap of an in-vacuum ID. We describe the experimental challenges in mapping the field of an 80 mm period in-vacuum wiggler, IVW80, using the vibrating wire technique, and compare results against simulation and data obtained from Hall probe measurements.

BACKGROUND

The vibrating wire [1] is an established measurement technique with widely reported use in aligning quadrupoles and probing ID error fields [2]. However, relatively little work has been reported on mapping an entire ID field with a wire, as this is generally achieved via Hall probe scan [3].

THEORY

Vibrating wire measurements make use of the following differential equation, which relates the wire's transverse displacement $u = u(t,z)$ to driving force $F(t,z)$:

$$\mu u_{tt} + \gamma u_t - T u_{zz} = F(t,z) \qquad (1)$$

for longitudinal coordinate z and time t. Here, the subscripts denote partial derivatives, e.g. $u_t = \delta u/\delta t$. The coefficients of the differential terms are: linear mass density μ, damping factor γ, and wire tension T.

If the wire is fixed at end points that extend beyond the magnetic field under measurement, $B(z)$, the solution to Eq. (1) is constrained such that it can be expressed as a Fourier sine series. Assuming $F(t,z)$ results from the magnetic field, the field can similarly be expressed as:

$$B(z) = \sum_{n=1}^{\infty} B_n \sin\left(\frac{n\pi}{L} z\right) \qquad (2)$$

where L is the distance between the wire's fixed points. If a sinusoidal current is used to drive the wire, then together with the magnetic field this results in a Lorentz force that serves as $F(t,z)$. (In this review, we neglect gravity's action upon the wire; see [1].)

From Eq. (1), the Lorentz force acting upon the wire, and thus the magnetic field, can be determined from a measurement of transverse displacement. To that end, one can sample the wire position at $z = z_s$.

In the case of a weakly damped wire, the transverse displacement is effectively zero for any sinusoidal driving force, save for when the wire is driven near its resonant frequency or integer multiples thereof. In short, when an appropriate drive frequency is chosen, the wire samples $B(z)$ at a point in frequency space corresponding to a particular wire harmonic n.

Consider now a time-average of $u(t,z)$ and current $I(t)$, which we denote by $\digamma_n(\omega)$ for harmonic n. We express the time-average function in two forms:

$$\digamma_n(\omega) = \frac{|u|I_0}{2}\cos\phi = \frac{B_n I_0^2}{2\mu}\sin\left(\frac{n\pi}{L}z_s\right)\frac{(\omega_n^2-\omega^2)}{\gamma'^2\omega^2+(\omega_n^2-\omega^2)} \quad (3)$$

where ϕ is the phase shift between $u(t,z)$ and $I(t)$ and $\gamma'=\gamma/\mu$. The first form is obtainable from observables, namely wire displacement u and phase ϕ. The second form predicts the shape of $\digamma_n(\omega)$ from wire parameters (μ, γ, T), drive current I_0, sensor position z_s, drive frequency ($\omega_n - \omega$), and magnetic field B. One can measure $\digamma_n(\omega)$ per the first form of Eq. (3) and fit a curve per the modified second form, Eq. (4). Ultimately, a series of B_n coefficients can be obtained using Eq. (5), where a_n are the fit coefficients of $\digamma_n(\omega)$ for all measured wire harmonics.

$$\digamma_n(\omega) = a_n \frac{(b_n-\omega^2)}{c_n\omega^2+(b_n-\omega^2)} + d_n \qquad (4)$$

$$B_n = a_n \frac{2\mu}{I_0^2}\sin\left(\frac{n\pi}{L}z_s\right)^{-1} \qquad (5)$$

EXPERIMENT

Hardware and Instrumentation

We drove a 0.1 mm diameter BeCu wire using a Keysight 33220A function generator and a SRS CS580 constant current source. The Keysight served as master oscillator for our system, selected for its sub-Hz resolution even at high drive frequency (>10 kHz).

We observed the wire vibration using a single Motorola H2A1 photogate, selected for its widespread use in the literature. Our system required careful setup to mitigate noise in the photogate signal, which initially dominated the measurement. We ran the photogate output through an AC-60B bridging transformer and measured the noise-isolated signal with a Signal Recovery 7265 dual phase DSP lock-in amplifier, which also measured the wire phase relative to the drive signal.

From measurements of the wire's physical parameters (omitted here for brevity) we calculated its resonant frequency to be 50.77 ± 0.91 Hz. The lowest observed resonance occurred at 51.6 ± 0.1 Hz, matching expectation to within experimental uncertainty. Note that the wire's fundamental frequency was sensitive to changes in ambient temperature on the order of 1 Hz °C⁻¹, and very

_____
† cameron.baribeau@lightsource.ca

high wire harmonics were thus extremely sensitive. We controlled ambient temperature to within ± 0.1 °C, but otherwise applied no temperature based correction.

Simulation and Independent Measurement

Reference Hall probe (HP) data were acquired in a 2015 factory acceptance test with the ID supplier. While IVW80's magnets were open to atmosphere during the vibrating wire (VW) measurements, mechanical supports prevented transverse access. Due to an oversight on our part, the 2015 HP and 2019 VW measurements were taken at different magnetic gaps (5.2 and 6.0 mm, respectively). The latter gap was not recorded directly but rather inferred from comparison against a calibrated model.

We simulated IVW80 in RADIA [4], which was critical to inform the regions of interest for measurement. Figure 1 shows the simulated magnetic field across the ~3.5 m wire length (top) as well as the Fourier sine transformation thereof, plotted versus wire harmonic number (bottom).
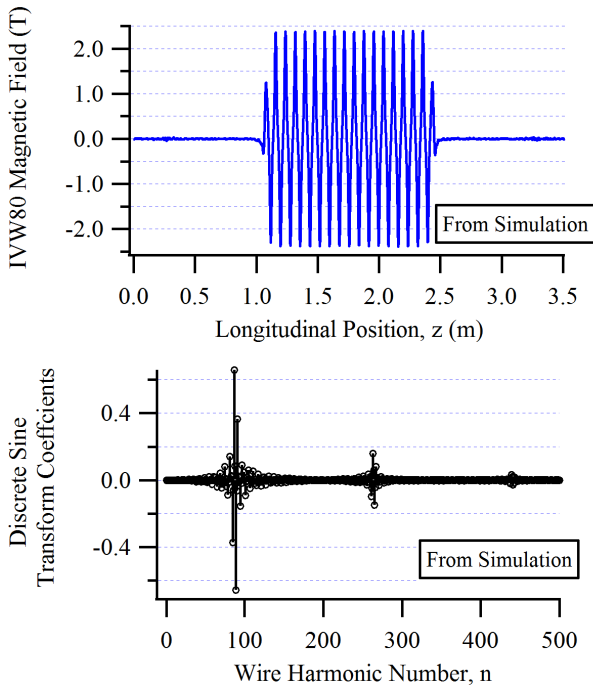
Figure 1: Predicted magnetic field (top) and Fourier sine transform thereof (bottom) of IVW80 at 6.0 mm gap.

The clustering of series coefficients near n ≈ (91, 273, 455) correspond to the 1st, 3rd, and 5th Fourier harmonics of the IVW80 field. Since the wire extends beyond the central (periodic) wiggler field, the overall series resembles a windowed sinusoid, where windowing disperses the series coefficients by way of spectral leakage. If the wire were centered on the ID, a modelled (errorless) field would consist strictly of odd wire harmonics, and even wire harmonics would indicate an error term in the measurement [5]. We did not sufficiently center IVW80 relative to the wire end clamps (~2 mm offset), and so even harmonics do not solely indicate field errors.

Measurement and Data Analysis

We developed automation in-house to sweep the drive frequency and capture the wire's magnitude and phase. Based on the predicted sine series, we selected 245 harmonics for measurement. Data were captured over ~3.5 days of continuous scan time, averaging 10 samples at each frequency, and idling 0.1 s between samples. Figure 2 shows data for the strongest (n = 91) harmonic.

Several modes had to be re-measured at lower drive current, as we overdrove the wire, which results in non-planar motion divergent from the theoretical model established above. We observed good results by restricting the wire displacement to 25 µm or less, noting that as the drive frequency increases, the onset of non-planar motion occurs at ever smaller vibration amplitude [6]. Ultra-high harmonics (n > 400) were restricted to 1 µm or less, which challenged the limits of our signal-to-noise.
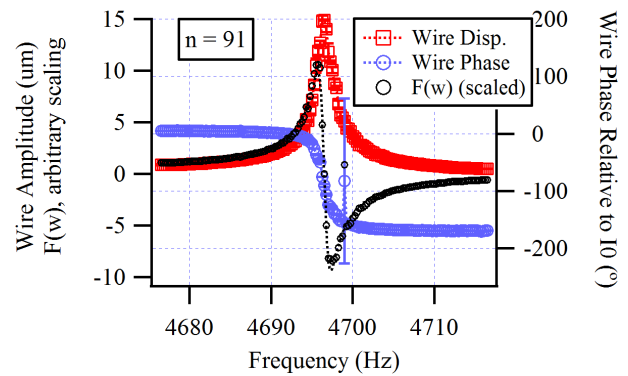
Figure 2: Observed magnitude, phase, and calculated $\mathcal{F}_n(\omega)$ for vibrations at the 91st wire harmonic.

Given the size of our data set, it was important to develop a fitting algorithm that worked well across hundreds of curves. Table 1 lists the initial values and constraints selected for fitting to $\mathcal{F}_n(\omega)$. Attempts to fit to the wire vibration amplitude, rather than $\mathcal{F}_n(\omega)$, yielded a less accurate field reconstruction, with particular trouble processing the even wire harmonics.

Table 1: Initial Values and Constraints for $\mathcal{F}_n(\omega)$ Fitting

Coeff.	Physical Meaning	Initial Value	Constraint
a	Amplitude	10^4	None
b	Resonant Frequency	ω of Max $\delta\mathcal{F}_n(\omega)/\delta\omega$	None
c	Damping Term	1	0 < c < 2.5
d	Offset	0	-1 < d <1

It is implicit in the theory of this technique that a given wire resonant mode should occur at ± 90 ° phase offset between the wire vibration and drive current. In practice, we often observed wire harmonics occurring 10-60 ° away from the expected value. We attributed this to an

unidentified hardware phenomenon and applied a correction factor to force ϕ to $\pm 90°$ for each harmonic.

Experimental Error

We considered two main error types in our measurement of IVW80. First, a basic propagation of calculus-based measurement uncertainty (of wire parameters, fitting uncertainty, etc.) into B_n coefficients can be expressed as:

$$\delta B_n = B_n \left[\frac{\delta a_n}{a_n} + \frac{\delta \mu}{\mu} + 2 \frac{\delta I_0}{I_0} + k_n z_s \cot(k_n z_s) \left(\frac{\delta L}{L} + \frac{\delta z_s}{z_s} \right) \right] \quad (6)$$

where $k_n = n\pi/L$ denotes the spatial frequency of the wire.

Second, there is error implicit in our finite, i.e. truncated, data set. Our photogate sampled the wire displacement at fixed z_s, which for some harmonics landed close to or upon a vibrational node; consequently, several modes were lost due to lack of detectable signal. We also overlooked small but nontrivial modes around n = 210…245. The overall truncation error is approximated based on the strengths of the missing wire harmonics per the simulated sine series.

Figure 3 shows the signal from each error type, as well as their sum, across the wire. Each error has a peak strength of roughly ± 0.1 T, albeit the truncation error contributes more strongly near the field terminations (± 0.2 T).

Truncation error could be eliminated by capturing more harmonics and adjusting the sensor position. Reducing measurement error is more challenging. Our current source reports an accuracy of $\pm 0.5\%$ (δI_0), and in our 10-sample measurements of wire position we consistently observed a standard deviation of $\approx \pm 3\%$, which factors into δa_n.
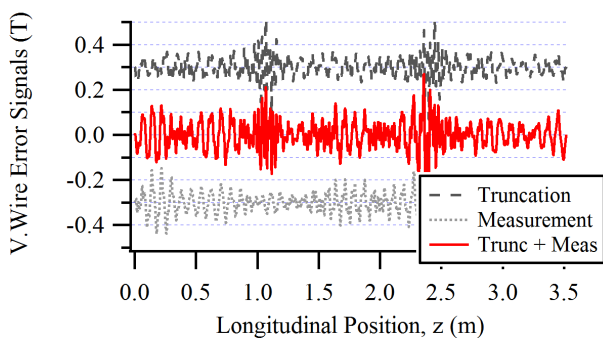
Figure 3: Error in reconstructed field due to measurement uncertainty and omitted wire harmonics, i.e. truncation.

Results

Figure 4 shows the field map of IVW80 reconstructed from the VW data set. Figure 5 shows peak magnetic field from the VW, the 2015 HP data, and as predicted in RADIA. We numerically scale the HP data from 5.2 mm to 6.0 mm gap per the dependence $e^{-\pi \, gap / \lambda}$, i.e. a relative factor of 0.969. The disagreement between HP data and RADIA simulation suggests a miscalibration in either the gap dependence of the model or the numerical scaling of the HP data.

The RADIA model is tuned to agree within 0.01% of the 2015 HP data's average peak field at 5.2 mm gap. At 6.0 mm gap, the model predicts a K-parameter of 17.74 and

~1.5% variation in peak-to-peak field. The VW data found an average K-parameter of 17.96 (1.2% disagreement) and ~4% peak-to-peak field variation.
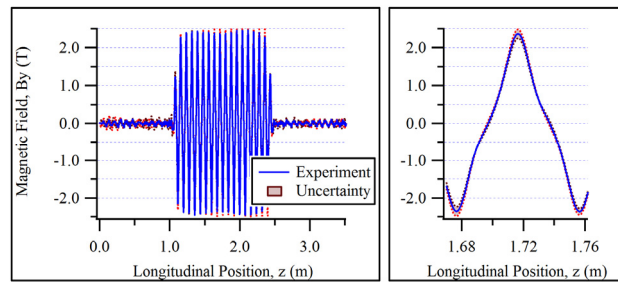
Figure 4: IVW magnetic field reconstructed from vibrating wire measurement, with one central period shown at right.
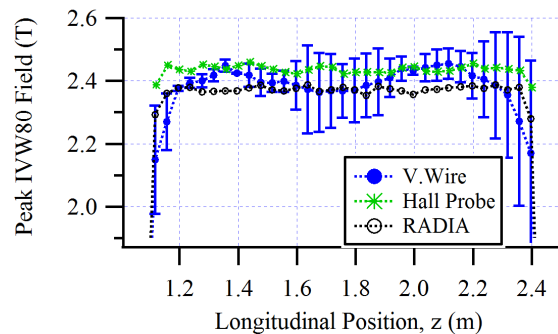
Figure 5: IVW80 magnetic field peaks from vibrating wire, Hall probe, and RADIA simulation. Dashed lines indicate bounds of experimental error in VW data (per Fig. 3).

CONCLUSION

The vibrating wire technique has historically been reserved as a supplemental tool for the Hall probe. It is a technical challenge for the vibrating wire to match the Hall probe as a field mapping technique, requiring a very stable current and signal generator from $\approx$ 1-30,000 Hz.

In this discussion, we showed an $\approx$ 80hr continuous vibrating wire scan that is less accurate than typical Hall probe results. The vibrating wire scan could be made several times faster by reducing the number of averaged samples or shortening the time delay between measured frequencies. Regardless, in situations where Hall probe access is difficult or impossible, measurement hardware has progressed such that a full field map of an ID, accurate to at worst a few percent, is indeed achievable with the vibrating wire.

REFERENCES

[1] A. Temnykh, "Vibrating wire field-measuring technique", *Nucl. Instrum. Methods Phys. Res.,* Sect. A, vol. 622, pp. 650-656, 2010.

[2] Z. Wolf, "A vibrating wire system for quadrupole fiducialization", SLAC, California, USA, 2005.
http://www.slac.stanford.edu/pubs/slactns/tn04/slac-tn-10-087.pdf

[3] A. Temnykh, Y. Levashov, and Z. Wolf, "A study of undulator magnets characterization using the vibrating wire

technique", *Nucl. Instrum. Methods Phys. Res.,* Sect. A, vol. 622, pp. 650-656, 2010.

[4] P. Elleaume, O. Chubar, and J. Chavanne, "Computing 3D magnetic fields from insertion devices", in *proc. PAC97*, Vancouver, Canada, 1997, paper 9P027, pp. 3509-3511.

[5] A. Temnykh, "Vibrating wire apparatus for periodic magnetic structure measurement", *Nucl. Instrum. Methods Phys. Res.,* Sect. A, vol. 515, pp.387-393, 2003.

[6] H. Pedersen and J. Knudsen, "Direct determination of the non-linear connection between tension and transverse amplitude for a vibrating string", *European Journal of Physics*, vol. 38, no. 4, p. 045003, 2017.